2010

Modeling the noble metal/TiO_2 (110) interface with hybrid DFT functionals: A periodic electrostatic embedded cluster model study

Salai Cheettu Ammal
University of South Carolina - Columbia, ammal@cec.sc.edu

Andreas Heyden
University of South Carolina - Columbia, heyden@cec.sc.edu

Publication Info

Published in *Journal of Chemical Physics*, Volume 133, Issue 164703, 2010.

Modeling the noble metal / TiO 2 (110) interface with hybrid DFT functionals: A periodic electrostatic embedded cluster model study

Salai Cheettu Ammal and Andreas Heyden

Citation: The Journal of Chemical Physics **133**, 164703 (2010); doi: 10.1063/1.3497037
View online: http://dx.doi.org/10.1063/1.3497037
View Table of Contents: http://scitation.aip.org/content/aip/journal/jcp/133/16?ver=pdfcov
Published by the AIP Publishing

Modeling the noble metal/TiO_2 (110) interface with hybrid DFT functionals: A periodic electrostatic embedded cluster model study

Salai Cheettu Ammal and Andreas Heyden[a)]
Department of Chemical Engineering, University of South Carolina, 301 S. Main St., Columbia, South Carolina 29208, USA

(Received 12 April 2010; accepted 14 September 2010; published online 26 October 2010)

The interaction of Au_n and Pt_n (n=2,3) clusters with the stoichiometric and partially reduced rutile TiO_2 (110) surfaces has been investigated using periodic slab and periodic electrostatic embedded cluster models. Compared to Au clusters, Pt clusters interact strongly with both stoichiometric and reduced TiO_2 (110) surfaces and are able to enhance the reducibility of the TiO_2 (110) surface, i.e., reduce the oxygen vacancy formation energy. The focus of this study is the effect of Hartree–Fock exchange on the description of the strength of chemical bonds at the interface of Au/Pt clusters and the TiO_2 (110) surface. Hartree–Fock exchange helps describing the changes in the electronic structures due to metal cluster adsorption as well as their effect on the reducibility of the TiO_2 surface. Finally, the performance of periodic embedded cluster models has been assessed by calculating the Pt adsorption and oxygen vacancy formation energies. Cluster models, together with hybrid PBE0 functional, are able to efficiently compute reasonable electronic structures of the reduced TiO_2 surface and predict charge localization at surface oxygen vacancies, in agreement with the experimental data, that significantly affect computed adsorption and reaction energies. © *2010 American Institute of Physics*. [doi:10.1063/1.3497037]

I. INTRODUCTION

The metal-oxide interface plays a crucial role in a variety of areas in nanomaterial science such as microelectronics, catalysis, and photonics.[1] Since Haruta[2] and Goodman and co-workers[3] discovered the extraordinary catalytic properties of nanosized Au particles, extensive research has been focused on this area.[4] The unique catalysis by Au nanoparticles[5] has, in most cases, been attributed to the three-phase boundary (TPB) of a gas-phase, small metal particle and a reducible oxide support, and it has been suggested by Haruta[6] that the mechanism of gold catalysis at the TPB can also be applied to other noble metals such as Pt. Thus, understanding the nature of the interactions at the metal-oxide interface is of utmost importance for the rational design of this new class of catalysts, whose activity and selectivity are primarily determined by the TPB of oxide supported noble metals. An industrially relevant reaction system constitutes the interface of Au and Pt clusters deposited on the rutile TiO_2 (110) surface. These catalytic systems are known to be highly active for many heterogeneous catalytic reactions including partial oxidation,[7] partial hydrogenation,[8] and the water-gas shift reaction[9,10] (WGS) ($CO+H_2O \rightleftharpoons CO_2+H_2$).

The structural and electronic properties of Au/TiO_2 (110) and Pt/TiO_2 (110) systems have recently been studied extensively using a wide variety of experimental techniques. These include atomic force microscopy,[11,12] high-resolution electron microscopy,[11,13] x-ray photoelectron spectroscopy,[12,14–16] ultraviolet photoemission spectroscopy,[15,17] transmission electron microscopy,[18] and scanning tunneling microscopy.[3,19,20] While Pt/TiO_2 has been the prototype system for strong-metal-support interaction where the reactivity of the metal particle is strongly modified by the presence of the support either by an electronic interaction between the metal and the support or by a chemical exchange that leads to the encapsulation of Pt clusters by reduced oxides,[16,20,21] Au/TiO_2 does not undergo significant encapsulation under equivalent annealing conditions.[22] In addition to experimental techniques, computational methods based on density functional theory (DFT) calculations have become a powerful research tool for investigating the geometric and electronic properties of metal-oxide interfaces. The common computational approach for this study employs the conventional unit cell model with periodic boundary conditions. The calculations are performed with pure density functionals within the generalized gradient approximation (GGA) where the valence electronic states are expanded in a set of periodic plane waves. The preference of this approach for the description of the catalyst surface is due to the computational efficiency of plane wave codes that naturally take the translational symmetry of the system into account. However, because of the periodicity of adsorbents and defects, often very large unit cells are necessary to minimize the effect of the interaction between adsorbents and defects, which significantly increases the computational resource needs for these studies. Furthermore, various studies[23–25] have recently shown that hybrid DFT functionals that contain a certain percentage of Hartree–Fock exchange are essential for the accurate description of the electronic structure of nonmetallic solid materials in general and of oxygen defects in metal oxides in particular. However,

[a)]Author to whom correspondence should be addressed. Electronic mail: heyden@cec.sc.edu.

periodic DFT calculations with hybrid DFT functionals are still hardly affordable except for very small unit cells.

To circumvent some of these computational issues, we have used, in the present study, the computationally highly efficient embedded cluster model approach to investigate the interaction of small Au and Pt clusters on stoichiometric and partially reduced TiO_2 (110) surfaces. In particular, we used the periodic electrostatic embedded cluster method (PEECM) (Ref. 25) functionality that has recently been implemented in the TURBOMOLE program package.[26] The PEEC method provides electronic embedding of a finite quantum mechanical cluster in a periodic infinite array of point charges. Unlike electrostatic embedding with a finite set of point charges, the PEEC method takes advantage of the recent developments[27] in the periodic fast multipole method to provide the correct Madelung potential due to a periodic array of point charges. This PEECM approach with hybrid DFT functional has recently been employed to study point defects in CaF_2 and CeO_2, and with a careful selection of the quantum cluster model, an accurate description of the atomic and electronic structures could be obtained for both the defect-free and defective surfaces.[25]

One of the most common point defects observed on the rutile TiO_2 (110) surface is a bridging oxygen vacancy, which significantly affects the surface chemistry and electronic properties of this material. Experimental observations indicate that removing bridging oxygen atoms from the TiO_2 surface produces a localized state approximately 0.8 eV below the conduction band.[28] The corresponding excess electron density is thought to be localized on the pair of Ti atoms neighboring the vacancy. Due to the well known self-interaction error of standard GGA-DFT, these methods produce delocalized holes and electrons on the defective TiO_2 surface. Recent studies have shown that these deficiencies can be corrected with the help of hybrid functionals[24,29,30] or the DFT+U approach.[30,31] Both methods also predict a much wider band gap than GGA-DFT functionals, which is again in much better agreement with the experimental observations. Although it seems that these approaches can provide a better electronic structure of the defective surface, it is still not clear as to what extent they affect the interaction of metal clusters on these surfaces. Here, we have investigated the effect of Hartree–Fock exchange on the description of the strength of chemical bonds at the interface of Au/Pt clusters and the TiO_2 (110) surface. We studied the interaction of Au_n and Pt_n (n=2–3) clusters on the stoichiometric and partially reduced TiO_2 (110) surfaces using the PEECM approach and compared the results to those obtained from standard GGA-DFT functionals and periodic slab models. We note that we decided not to use the DFT+U approach for this study, although it seems to be a practical way to improve the electronic structure of reduced oxide surfaces, since there is currently very limited experience on the transferability of the "U" parameter from a nondefective to a defective system and the determination of the "U" parameter is likely very dependent on the particular system and/or property of interest.

This paper is organized as follows. After describing the models and summarizing the computational details in Sec. II, the computational results are discussed in Secs. III–V. The performance and accuracy of the PEEC methodology has been validated in Sec. III based on Pt adsorption and oxygen vacancy formation energies. Furthermore, we also investigated the effect of different DFT methods, including the double-hybrid density functional, on the Pt adsorption energy in order to choose an appropriate DFT method for our present investigation. A detailed investigation on the adsorption of Au and Pt dimers and trimers on the stoichiometric and reduced TiO_2 (110) surface is made in Sec. IV, and the effect of the metal clusters on the reducibility of TiO_2 (110) surface is analyzed in Sec. V. Finally, conclusions are summarized in Sec. VI.

II. COMPUTATIONAL DETAILS

A. Periodic DFT calculations

A periodic slab model is required to build and validate a periodic electrostatic embedded cluster model. All periodic DFT calculations presented here have been performed using the VASP 4.6 program.[32] We choose the Perdew–Burke–Ernzerhof (PBE) (Ref. 33) functional within the generalized gradient approximation to describe the exchange and correlation effects. The number of valence electrons considered for Ti, O, Au, and Pt are 10, 6, 11, and 10, respectively. The bulk rutile TiO_2 has a tetragonal structure with two TiO_2 units per unit cell. The calculated PAW-PBE lattice constants, $a=4.649$ Å and $c=2.971$ Å, are in close agreement with the experimental values of 4.593 and 2.958 Å. These lattice parameters were used to construct stoichiometric (2×1) and (4×2) supercell (110) surface slabs with 12 atomic layer thickness. A vacuum gap of 17 Å was found to give converged adsorption energies. A $(2\times2\times1)$ Monkhorst–Pack k-mesh with an energy cutoff of 400 eV was used for structure relaxations. The k-mesh was increased to $(4\times4\times1)$ whenever the smaller (2×1) supercell was used. Monopole, dipole, and quadrupole corrections to the energy were taken into account using a modified version of the Markov and Payne method.[34] Harris–Foulke-type corrections[35] have been included for the forces. Finally, fractional occupancies of bands were allowed using a window of 0.05 eV and the Gaussian smearing method. All atoms in the solid and the clusters were relaxed except for the bottom 3 atomic layers of the TiO_2 (110) slab, which were fixed at their bulk positions to mimic bulk behavior. For all Au_n and Pt_n adsorption studies, the metal clusters were allowed to adsorb only on the relaxed side of the TiO_2 surface. All calculations have been performed spin-polarized and no symmetry restrictions have been imposed during the geometry optimizations. The energies of the isolated Au_n and Pt_n clusters were calculated at the Γ point in a 12 Å cubic supercell. In order to avoid artifacts in the electronic structure derived from nonrelaxed atoms, density of states (DOS) calculations have been performed from fully relaxed structures using the tetrahedron method with Bloch corrections and a k-point grid enlarged to $4\times4\times2$.

B. Periodic electrostatic embedded cluster calculations

PEECM calculations have been performed on a range of neutral $(TiO_2)_n$ cluster models, employing the PBE exchange-correlation functional[33,36] and its hybrid modification PBE0 (Ref. 37) also called PBEh. To speed up the calculations using the PBE functional, the resolution of identity approximation has been applied for the Coulomb potentials.[38] The TURBOMOLE 6.0 program package[39] is used for all PEECM calculations. The selection of the cluster models used in this study is explained in Sec. III. All clusters have been embedded in a periodic field of point charges (+4 for Ti and −2 for O). In order to avoid spurious polarization of the outer cluster oxygen atoms, positive point charges representing Ti atoms nearest to the cluster model have been represented by total ion model potentials (TIMPs), which consist of a +4 charge and a Ti^{4+} effective core potential (ECP).[40] Our reasons for using formal charges instead of lower point charges (e.g., +2/−1 for Ti/O) as used in previous studies[41–43] employing embedded cluster models are discussed in Sec. III A. A surface slab unit cell with 30 atomic layers thickness optimized with the VASP program has been used to define the periodic field of point charges for the PEECM calculations. The slab thickness has been systematically increased to yield converged HOMO-LUMO gaps (convergence criterion: 10^{-3} eV), vacancy formation energies (convergence criterion: 10^{-3} eV), and Pt adsorption energies (convergence criterion: 10^{-4} eV). The cluster Ti and O atoms were represented by the all-electron TZVP basis set.[44] Au and Pt were represented by relativistic small core ECPs (Ref. 45) together with a TZVP basis for the valence electrons. The positions of Au_n, Pt_n, and all Ti and O atoms in the cluster model (except those directly connected to the TIMPs) have been relaxed during geometry optimizations. Also, the DOS for the clusters are obtained using Gaussian smearing of Kohn–Sham orbital energies.

Adsorption energies of M_n (M=Au, Pt) clusters, $E_{ads}[M_n]$, on the stoichiometric (S-TiO_2) or reduced (R-TiO_2) surface are obtained using

$$E_{ads}[M_n] = E[M_n/TiO_2] - E[TiO_2] - E[M_n], \quad (1)$$

where $E[M_n/TiO_2]$ and $E[TiO_2]$ are the total energies of stoichiometric or reduced TiO_2 with and without the metal cluster on its surface, respectively, and $E[M_n]$ is the total energy of the metal cluster at its minimum energy configuration in the gas phase. All the adsorption energies have been corrected for the basis set superposition error (BSSE) with the counterpoise method,[46] unless stated otherwise. The surface with an oxygen vacancy (R-TiO_2) has been calculated by removing a bridging oxygen atom and retaining the "ghost" basis set of oxygen at the vacancy.

To estimate the oxygen vacancy formation energy (E_{vf}) on the TiO_2 (110) surface, we used

$$E_{vf} = E[R\text{-}TiO_2] + \tfrac{1}{2}E[O_2] - E[S\text{-}TiO_2], \quad (2)$$

where $E[O_2]$ is the energy of a gas-phase oxygen molecule. In order to avoid difficulties associated with the GGA-DFT treatment of the triplet state of gas-phase O_2,[47] the O_2 energies are obtained from the H_2O splitting reaction [Eq. (3)] using the experimental reaction energy and calculated DFT energies of H_2 and H_2O in the gas phase,[48]

$$E_{O_2}^{tot} = 2[(E_{H_2O}^{DFT} + E_{H_2O}^{ZPE}) - (E_{H_2}^{DFT} + E_{H_2}^{ZPE}) - E_{hof}] - E_{O_2}^{ZPE}, \quad (3)$$

where the experimental zero point energies (E^{ZPE}) of H_2O, H_2, and O_2 are 0.558, 0.273, and 0.098 eV, respectively.[49] E_{hof} is the experimental heat of formation of a gas-phase H_2O molecule (−2.505 eV),[49] and E^{DFT} is the energy calculated with the PBE functional. For reaction energies calculated with the PBE0 functional, we used the O_2 energy as obtained from our present calculations without such a correction since the calculated oxygen binding energy using the PBE0 functional (−5.24 eV) agrees well with the experimental value (−5.12 eV).[50]

III. VALIDATION OF THE PEEC MODELS

A. Adsorption of Pt on the stoichiometric TiO_2 (110) surface

The structure of the top layers of the TiO_2 (110) surface is shown in Fig. 1(a). The surface is composed of atoms with different local environments such as five- and sixfold coordinated Ti atoms (Ti_{5c} and Ti_{6c}), threefold coordinated surface oxygen atoms (O_s), and doubly coordinated bridging oxygen atoms (O_b). The present study involves the adsorption of metal clusters and the presence of oxygen vacancies on the TiO_2 (110) surface. In order to assess the performance of the PEEC methodology and to choose an appropriate cluster model for this study, we chose a range of neutral $(TiO_2)_n$ cluster models and tested their suitability by comparing the Pt monomer adsorption energies and the oxygen vacancy formation energies with those obtained from periodic slab models. The adsorption of a Pt atom on two different sites, the H [fourfold hollow site over Ti_{5c}, Fig. 1(b)] and T sites [on top of O_s, Fig. 1(c)], was considered for this comparison. These two sites were reported to be the most stable adsorption sites for Pt on the TiO_2 (110) surface. Figures 1(d)–1(g) illustrate the cluster models used for this Pt monomer adsorption study. The calculated adsorption energies for the periodic slab and PEEC models are listed in Table I. Pt adsorption energies for the hollow site (H), obtained from the periodic slab models, agree well with the previously reported values by Iddir *et al.*[51,52] These authors predicted, using the PW91 functional,[36] that Pt adsorption on the hollow site (H) is more stable than Pt adsorption on top of a surface oxygen atom (T). Although our periodic slab calculations with PBE functional predict the adsorption of Pt at the T site to be more favorable, the adsorption energy difference for the H and T sites is less than 0.1 eV. Furthermore, the results illustrated in Table I suggest that adsorption energies calculated with the $Ti_{17}O_{34}$ model are converged with respect to cluster size to within 0.1 eV for the H site and 0.03 eV for the T site. The cluster models predict slightly larger adsorption energies (by about 0.3 eV) compared to the periodic slab models. Based

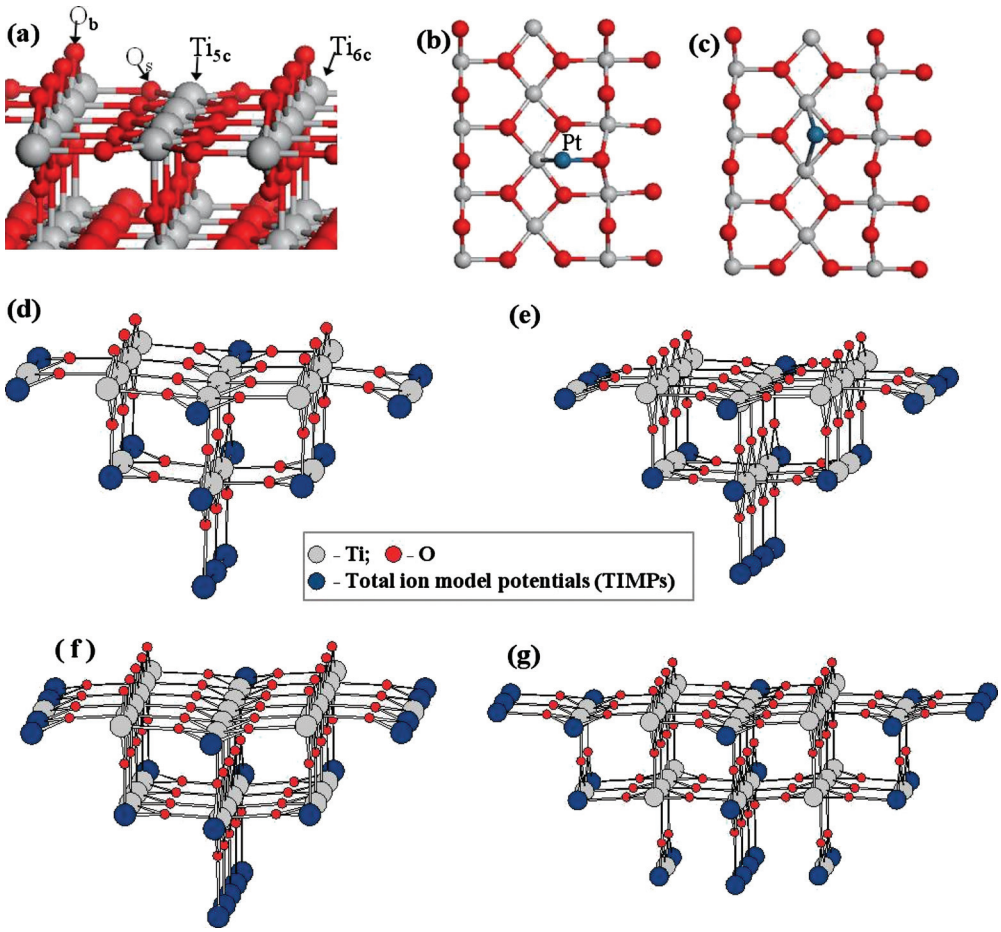

FIG. 1. (a) Stoichiometric rutile TiO_2 (110) surface. Atoms are labeled as follows: O_b—bridging oxygen atom; O_s—in-plane surface oxygen atom; Ti_{5c}—fivefold coordinated Ti atom; and Ti_{6c}—sixfold coordinated Ti atom. [(b) and (c)] TiO_2 (110) structures with an adsorbed Pt atom at the fourfold hollow site over Ti_{5c} (H) and on top of the surface O_s (T) site, respectively. [(d)–(g)] Cluster models used to study Pt adsorption on the TiO_2 (110) surface: (d) $Ti_{17}O_{34}$, (e) $Ti_{23}O_{46}$, (f) $Ti_{29}O_{58}$, and (g) $Ti_{33}O_{66}$.

on this cluster model convergence test, we consider all the investigated cluster models suitable for further adsorption studies.

The adsorption of single metal atoms, such as Cu,[42] Ag,[42] Au,[42] and Pd,[41,43] as well as the Pd dimer[41] on the TiO_2 (110) surface has been studied earlier using cluster models embedded in a *finite* array of point charges. A set of smaller point charges (+2/−1 for Ti/O) has been used for embedding in most cases. Moreover, Sanz *et al.*[43] tested the effect of various embedding point charges including different sets of fractional point charges for Pd adsorption on the TiO_2 (110) surface. In particular, they showed that the use of formal charges (+4/−2) for embedding makes the cluster too ionic, which leads to too much net charge transfer from the metal to the TiO_2 surface as well as too large adsorption energies. However, the cluster models used in these reports are significantly smaller than the cluster models used in the present study. Also, no surface relaxation was permitted in these earlier adsorption studies. To test the effect of point charges on our cluster models, we calculated the adsorption energies of Pt [at T position; Fig. 1(c)] on the models shown in Figs. 1(d)–1(f) using (+2/−1) and (+4/−2) point charges for the Ti/O atoms and an 18-electron ECP (Ref. 40) together with +2 and +4 charges for the TIMPs, respectively. For this set of calculations, we used the PBE functional and (as argued below) we allowed to relax the positions of only a limited number of Ti and O atoms in the cluster together with the Pt atom. The effect of point charges has been analyzed by comparing the HOMO-LUMO gap of the cluster, the Pt adsorption energy, and the charge on the Pt atom obtained from natural population analysis (NPA).[53] Table II illustrates that the adsorption energy and the charge on the Pt atom are overestimated by about 0.4 eV and 0.16 e, respectively, for

TABLE I. The calculated Pt adsorption energies (E_{ads}) on a TiO_2 (110) surface using different computational models.

Method	Model[a]	E_{ads} (eV) H[a]	E_{ads} (eV) T[a]
Periodic slab (PBE)	(2×1) surface cell	−1.83	−1.88
	(4×2) surface cell	−1.95	−2.00
PEECM (PBE)	$Ti_{17}O_{34}$+Ti_{15} (TIMPs)	−2.21	−2.29
	$Ti_{23}O_{46}$+Ti_{18} (TIMPs)	−2.31	−2.29
	$Ti_{29}O_{58}$+Ti_{21} (TIMPs)	−2.30	−2.26
	$Ti_{33}O_{66}$+Ti_{26} (TIMPs)	−2.29	−2.26

[a]Refer to Fig. 1. Adsorption energies for PEECM models are BSSE corrected, which changed the metal adsorption energy by less than 0.1 eV.

TABLE II. Effect of point charge field on the adsorption of Pt on $(TiO_2)_n$ cluster models calculated with PBE functional.

Cluster	Property	Point charges used for Ti/O (+2/−1)	(+4/−2)	Δ[a]
$Ti_{17}O_{34}$	HOMO-LUMO gap (eV)	−0.05	1.95	
	E_{ads} (Pt at T) (eV)[b]	−1.85	−2.29	0.44
	NPA charge on Pt	0.43	0.59	0.16
$Ti_{23}O_{46}$	HOMO-LUMO gap (eV)	0.07	1.82	
	E_{ads} (Pt at T) (eV)[b]	−1.93	−2.25	0.32
	NPA charge on Pt	0.47	0.56	0.09
$Ti_{29}O_{58}$	HOMO-LUMO gap (eV)	0.00	1.78	
	E_{ads} (Pt at T) (eV)[b]	−2.07	−2.24	0.17
	NPA charge on Pt	0.52	0.55	0.03

[a]Difference in property computed with two different sets of point charges.
[b]Adsorption energies are not corrected for BSSE.

the smaller cluster ($Ti_{17}O_{34}$) when using formal charges instead of the lower (+2/−1) point charges. However, this energy and charge difference decreases with an increase in the cluster size. For the larger $Ti_{29}O_{58}$ cluster, the difference in the adsorption energy is only 0.17 eV and the charge on the Pt atom is practically the same. Another important property is the HOMO-LUMO gap. While computations with formal charges predicted a HOMO-LUMO gap for all clusters in the range of 1.7–2 eV, which is in close agreement with the gap between occupied and unoccupied bands (1.7 eV) obtained from periodic slab calculations, the gap is nearly zero for clusters optimized with lower point charges. An upward shift of the molecular orbital energies and a very diffuse charge distribution of the highest occupied molecular orbitals have been observed whenever lower point charges were used. A similar trend in orbital energies with lower point charges was observed by Reinhardt *et al.*[54] in their CO adsorption study on TiO_2 (110) using a cluster model surrounded by multipoles. Such an electronic distribution slows down SCF convergence and leads to surprisingly unphysical structures if more than a very limited number of atoms in the cluster models are relaxed during optimization. Considering that no such problems have been observed whenever we used formal charges, all following PEECM calculations use formal charges with relatively large cluster models.

Next, we investigated the effect of different flavors of DFT on the Pt adsorption energy using the $Ti_{17}O_{34}$ cluster model. Table III illustrates that geometries obtained with various methods are very similar, suggesting that we are not required to use hybrid functionals for geometry optimizations but can use the computationally more efficient PBE functional. However, we note that this may not be the case for surfaces with vacant sites, where the description of the electronic structure is more dependent on the computational method. Table III further shows that adsorption energies calculated with the hybrid DFT functional PBE0 and the double-hybrid functional B2PLYP (Ref. 55) differ by less than 0.2 eV and are very close to those obtained with the (4×2) supercell periodic slab calculations, indicating that the PBE functional is able to correctly describe all interactions with the stoichiometric TiO_2 (110) surface. We note here that Grimme and co-workers[56] recently showed that the B2PLYP functional with at least triple-ζ quality atomic orbital basis sets has an accuracy that is competitive with the computationally very expensive coupled-cluster methods for transition metal complexes and noble metal clusters such as Au_8.[57] Finally, our calculations show that the popular B3LYP functional[55,58] significantly underestimates the adsorption energy by about 0.5 eV compared to the B2PLYP functional that has been shown[59] to provide a significantly improved accuracy. This again explains our selection of the hybrid PBE0 functional instead of the more commonly used B3LYP functional.

TABLE III. The calculated Pt adsorption energies (E_{ads}) on a TiO_2 (110) surface using the PEEC model with various flavors of DFT.

Model	Method	E_{ads} (eV) H[a]	T[a]
PEECM	PBE//PBE	−2.29	−2.39
$(Ti_{17}O_{34})$	B3LYP//PBE	−1.57	−1.60
	B3LYP//B3LYP	−1.59	−1.62
	PBE0//PBE	−1.85	−1.99
	PBE0//PBE0	−1.87	−1.99
	B2PLYP//PBE	−2.02	−2.12

[a]Refer to Fig. 1. Adsorption energies are not corrected for BSSE.

B. The partially reduced TiO_2 (110) surface

In the next step of our PEECM validation procedure, we focus on the partially reduced TiO_2 (110) surface with oxygen vacancies. The reduced surface is created by removing a bridging oxygen (O_b) atom from the surface. Upon removal of the O_b atom, the two Ti_{6c} atoms neighboring the oxygen vacancy become fivefold coordinated, which introduces structural and electronic changes in the first layer and subsurface atoms prohibiting the use of the cluster models illustrated in Figs. 1(d)–1(g). Instead, a different set of cluster models illustrated in Fig. 2 that are symmetric with respect to the bridging oxygen row has been selected for the study of oxygen vacancy formation energies. Again, the vacancy formation energy calculated with the periodic slab model (3.76 eV) is in good agreement with the previously reported values[31,60,61] for a similar oxygen vacancy concentration and supercell dimension. The PEECM results shown in Table IV indicate that the vacancy formation energy calculated with PBE functional decreases with increasing size of the cluster model and seems to converge to the value obtained with the periodic slab model for the $Ti_{46}O_{92}$ cluster. This observation can be explained by the tendency of the PBE functional to delocalize the excess charge produced by reducing the surface over Ti atoms in the subsurface layers instead of localizing them on the Ti atoms neighboring the vacancy. The extent of delocalization is maximized in the larger clusters, and thus larger reduced clusters are more stable than smaller reduced cluster. However, hybrid PBE0 calculations present a different picture. Figure 3 illustrates that the hybrid exchange functional fully localizes the excess charge on the Ti atoms neighboring the vacancy. A similar localization of

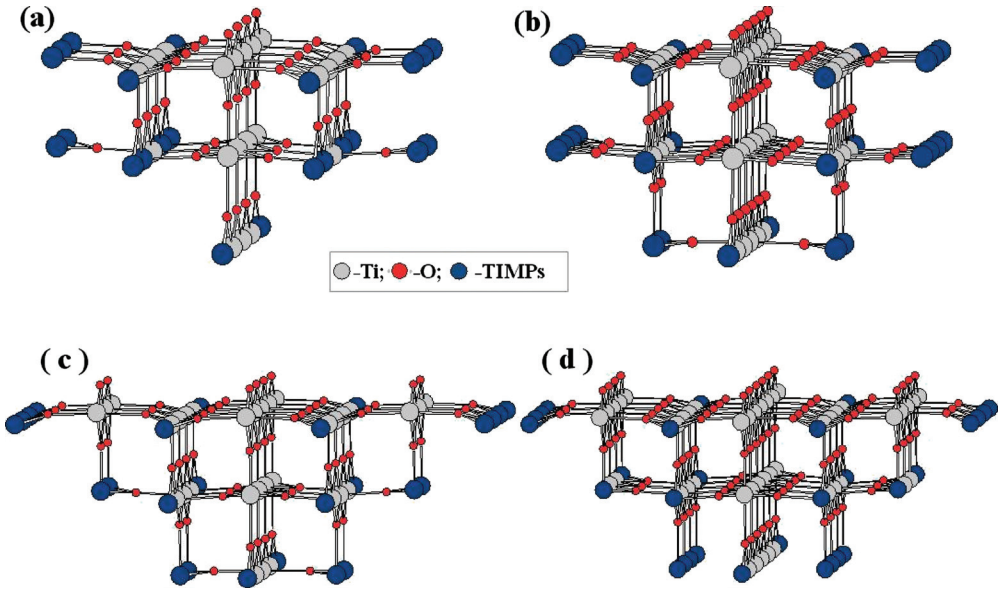

FIG. 2. Cluster models used to study the oxygen vacancy formation on TiO_2 (110) surfaces: (a) $Ti_{22}O_{44}$, (b) $Ti_{32}O_{64}(1)$, (c) $Ti_{32}O_{64}(2)$, and (d) $Ti_{46}O_{92}$.

charge density was observed for all symmetric clusters used for the calculation of vacancy formation energies (Fig. 2). The reduced cluster optimized with PBE0 functional is therefore less stable than the cluster optimized with PBE functional, i.e., the formation of an oxygen vacancy is more endothermic ($E_{vf} \approx 4.2–4.4$ eV) and the effect of cluster size is reduced due to localization of charge at the vacant site. E_{vf} slightly increases for the larger clusters with three bridging oxygen rows [Figs. 2(c) and 2(d)] because more atoms are allowed to relax in these clusters, which stabilize the nonreduced clusters. Overall, vacancy formation energies seem to be converged to within 0.1 eV for the largest clusters. Morgan *et al.*[31] reported a similar charge density localization for the reduced TiO_2 (110) surface using the DFT+U method and a periodic slab model. However, our results disagree with those of Di Valentin *et al.*,[24] who predicted localization at nonequivalent Ti_{5c} and Ti_{6c} sites when using the B3LYP functional.

Various test calculations by us with different cluster models showed that the size and symmetry of the cluster play a significant role in predicting localization of charge density on the surface. For instance, PBE0 calculations for the reduced clusters shown in Figs. 1(d)–1(f) predicted localization at nonequivalent Ti_{5c} and Ti_{6c} sites. The reasons for this prediction are that the oxygen vacancy in these clusters is too close to the embedding point charges and that the vacant site is surrounded by nonequivalent atoms. Whenever both points have been considered during the design of cluster models, localization of charge density at the vacant site has always been observed. Next, we note that the computation of the vacancy formation energy for a single vacant site has always been a problematic issue for periodic slab models because of the periodicity of defects on the surface. Previously reported values[62] highly depended on the slab thickness, the number of atomic layers kept fixed in their bulk positions, and the vacancy concentrations. All of these factors seem to have no influence on the calculations with cluster models and we believe that it is possible to calculate accurate vacancy formation energies for a single vacant site with the PEEC methodology and reasonably large clusters.

TABLE IV. Oxygen vacancy formation energies (E_{vf}) of a rutile TiO_2 (110) surface calculated with different cluster models.

Method	Model	E_{vf} (eV) PBE[a]	E_{vf} (eV) PBE0[b]
Periodic slab	(4×2) surface cell	3.76	···
PEECM	$Ti_{22}O_{44}+Ti_{24}$ (TIMPs)	4.04	4.18
	$Ti_{32}O_{64}(1)+Ti_{28}$ (TIMPs)	3.56	4.16
	$Ti_{32}O_{64}(2)+Ti_{26}$ (TIMPs)	4.04	4.27
	$Ti_{46}O_{92}+Ti_{30}$ (TIMPs)	3.75	4.37

[a]O_2 energy is calculated using Eq. (3).
[b]O_2 energy used to calculate E_{vf} is computed with the PBE0 functional without correction.

C. Cluster model for the metal-oxide interface

The results described above clearly indicate that the PEEC methodology, together with a careful selection of a cluster model, is able to reproduce both adsorption and oxygen vacancy formation energies. However, the cluster models shown in Fig. 1 are not suitable to model the reduced surface and the ones in Figs. 2(a)–2(c) are not suitable for the adsorption of more than one metal atom, considering that metal clusters adsorb on the TiO_2 (110) surface between two bridging oxygen rows. As a result, we chose the $Ti_{46}O_{92}$ cluster model [Fig. 2(d)] for further studies. Using the PBE functional, the calculated Pt adsorption energies (−2.12 eV at H site; −2.24 eV at T site) and the oxygen vacancy formation energy (3.75 eV) for this cluster are in good agreement with periodic slab model calculations. A similar test with this cluster and lower (+2/−1) embedding point charges, as described in Sec. III A, predicts a difference in Pt adsorption energy of less than 0.1 eV and almost no difference in the natural charge on Pt. Insight into the electronic

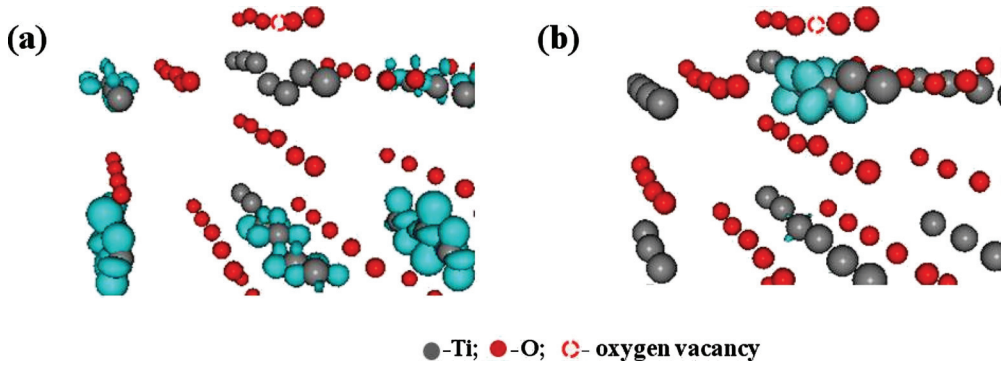

FIG. 3. Spin density distribution for the reduced $Ti_{32}O_{63}$(1) cluster optimized with (a) PBE and (b) PBE0 functionals. Density plots show the spin density isosurface of 0.02 e/Å^3.

structure of this embedded cluster can furthermore be obtained from the DOS. Figure 4(a) shows the total DOS (TDOS) of this cluster computed using the Mulliken population analysis with PBE and PBE0 functionals, together with the TDOS obtained from periodic slab model calculations (PBE functional). Both periodic DFT and PEECM calculations with PBE functional compute band gaps of 2.0 and 1.9 eV, respectively. In contrast, the cluster model calculations with the PBE0 functional yield a much wider band gap of 4.1 eV. Figure 4(b) illustrates the TDOS of the reduced surface ($Ti_{46}O_{91}$ cluster) with PBE and PBE0 functionals. The PBE calculation predicts a band gap of 2.1 eV and no gap state between the valence and the conduction bands. In contrast, the hybrid PBE0 calculation predicts a band gap of 4.0 eV and two gap states at 1.2 and 1.0 eV below the conduction band. Our PBE0 results are in reasonable agreement with the experimentally observed gap state 0.8 eV below the conduction band[63] and previous DFT+U (Ref. 31) and B3LYP calculations.[24] Although the hybrid PBE0 calculations overestimate the band gap of the TiO_2 surface by ~1 eV (the experimental value is ~3 eV), it allows us to visualize the localized states in the band gap and compare the position of these states to experimental observations. To conclude, it seems that the selected $Ti_{46}O_{92}$ cluster model, together with the hybrid PBE0 functional, is a reasonable surface model that has been used for all subsequent investigations.

IV. ADSORPTION OF Au_n AND Pt_n (n=2,3) CLUSTERS ON THE STOICHIOMETRIC AND REDUCED TiO_2 (110) SURFACE

The interaction of small Au clusters with the stoichiometric and reduced TiO_2 (110) surfaces has previously been investigated using periodic DFT methods.[64–66] For example, Chrétien and Metiu[60,67] reported a detailed investigation on the adsorption of Au_n (n=1–7) on the stoichiometric and partially reduced TiO_2 (110) surface based on structure, binding mechanism, and charge density distribution. Also, Madsen and Hammer[65] studied the effect of subsurface Ti interstitials on the bonding of small gold clusters on the rutile TiO_2 (110) surface, and Pabisiak and Kiejna[68] studied the adsorption of Au_n nanorows and Au_n clusters on the reduced TiO_2 (110) surface. In contrast, studies on the Pt/TiO_2 (110) system are scarce. Iddir *et al.*[51] studied the adsorption and diffusion of a single Pt atom on stoichiometric and reduced TiO_2 (110) surfaces and later discussed the interaction

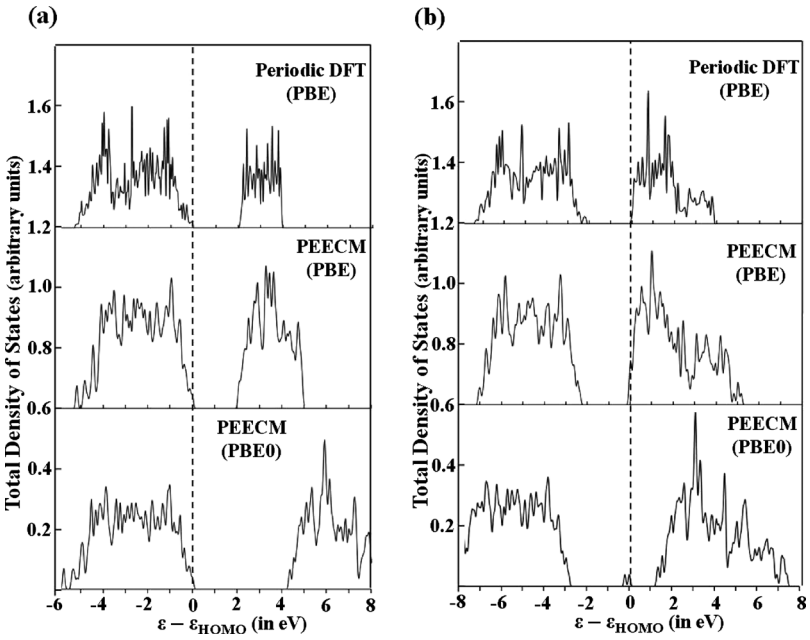

FIG. 4. (a) TDOS of the stoichiometric TiO_2 (110) surface computed using a periodic DFT code with PBE functional (on top), the PEEC method with PBE functional ($Ti_{46}O_{92}$ cluster; middle), and PEEC method with hybrid PBE0 functional (bottom). (b) The same as in (a) for the reduced TiO_2 (110) surface.

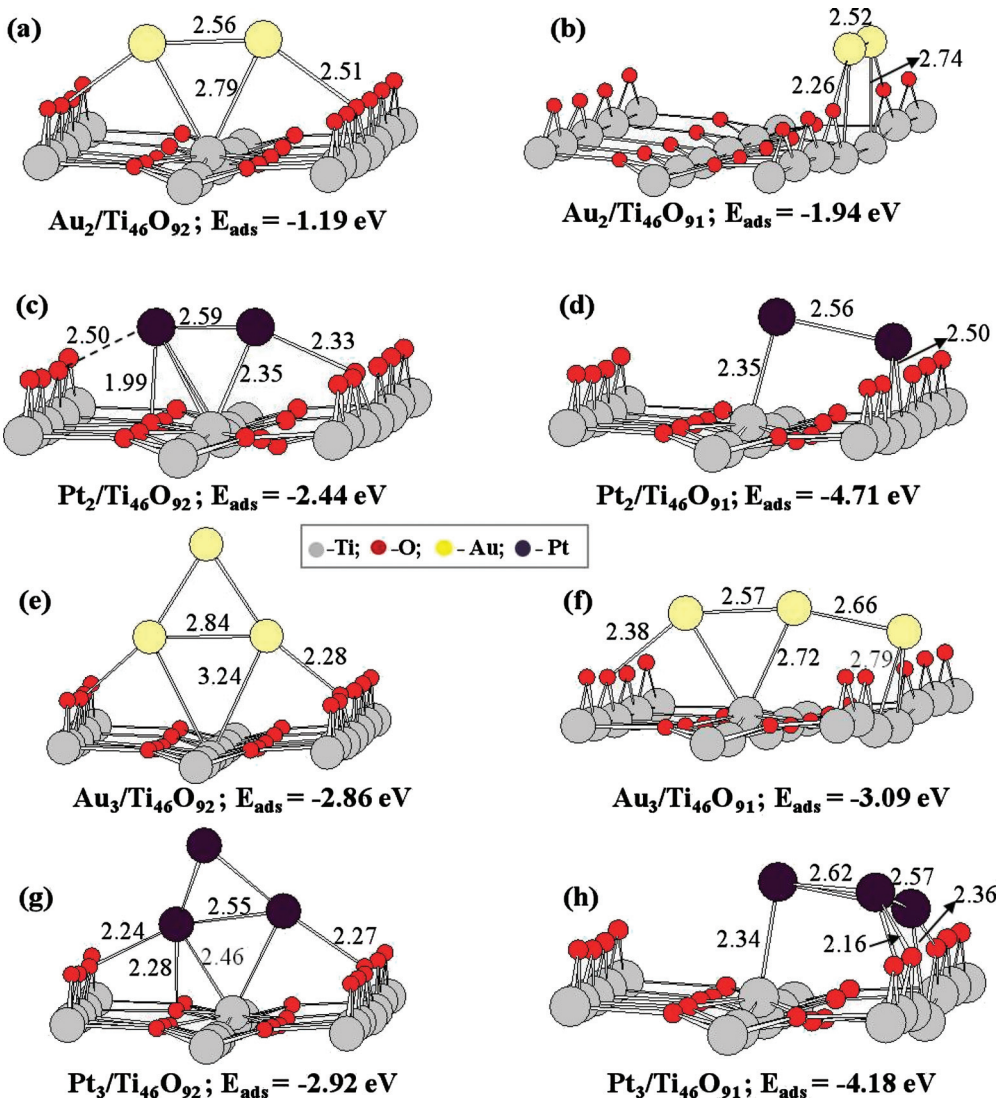

FIG. 5. Optimized structures, selected bond distances (in Å), and adsorption energies (in eV) of the M_n/TiO_2 surface calculated using the stoichiometric and reduced rutile TiO_2 (110) cluster model $Ti_{46}O_{92}/Ti_{46}O_{91}$ with PBE0 functional (only a part of the structure is given here for clarity).

of Pt_2 with the reduced TiO_2 (110) surface.[52] A few other reports were also made on the interaction of small Pt clusters with the anatase TiO_2 (101) surface.[69,70] All of these computational studies were done using periodic slab models with the GAA-PW91 or PBE functional. In this study, our focus has primarily been on the effect of hybrid exchange on these systems and to compare our results with those obtained with GGA functionals.

A. Adsorption energies and geometries of (M_n) clusters on the TiO_2 (110) surface

The lowest energy structures corresponding to the adsorption of Au_2, Pt_2, Au_3, and Pt_3 on the stoichiometric ($Ti_{46}O_{92}$ cluster) and reduced ($Ti_{46}O_{91}$ cluster) TiO_2 surface using the PBE0 functional are shown in Fig. 5. Various possible structures were considered for the geometry optimization in order to locate the minimum energy structure for each complex. The results suggest that the adsorption mode for all four clusters on the stoichiometric as well as reduced surface obtained with PBE0 functional is virtually identical to the results obtained with PBE functional. Table V lists the adsorption energies calculated for the Au and Pt dimer and trimer on the stoichiometric and reduced cluster models and periodic slab models with (4×2) supercell. The calculated adsorption energies for the Au_2 and Au_3 clusters on the periodic slab models agree well with values previously reported by Chrétien and Metiu using the PW91 functional.[60,67] In the case of adsorbed Pt complexes, Iddir *et al.*[52] computed a slightly stronger Pt_2 adsorption energy on the reduced TiO_2 surface (-3.62 eV versus -3.33 eV), which is likely the result of a different computational setup and the use of a different DFT functional.

Adsorption energies for the metal clusters on the stoichiometric surface calculated with the PEECM methodology and PBE functional are, except for the Au_3 cluster, within 0.3 eV to results from periodic slab calculations. For the Au_3 cluster, the energy difference between models is 0.8 eV. This large energy difference is expected to originate from a different delocalization of the excess charge on the TiO_2 surface computed by the periodic slab and PEEC models. The presence of an unpaired electron in a high-energy singly occupied molecular orbital of the Au_3 cluster stimulates a charge

TABLE V. Adsorption energies (E_{ads}) of Au and Pt clusters on stoichiometric and reduced TiO_2 (110) surface models.

			E_{ads} (eV)		
				PEECM ($Ti_{46}O_{92}$)[a]	
Surface	Metal	Ground state configuration	VASP (PBE)	PBE	PBE0
TiO_2	Au_2	Singlet	−0.97	−1.24	−1.19
	Au_3	Doublet	−1.68	−2.53	−2.86
	Pt_2	Singlet	−1.83	−2.10	−2.44
	Pt_3	Singlet	−3.15	−3.13	−2.92
TiO_{2-x}	Au_2	Triplet	−1.22	−1.16	−1.94
	Au_3	Doublet	−2.11	−2.51	−3.09
	Pt_2	Singlet	−3.33	−3.74	−4.71
	Pt_3	Singlet	−4.04	−3.73	−4.18

[a]BSSE corrections changed the metal adsorption energy by less than 0.1 eV/metal atom.

transfer from Au_3 to the TiO_2 surface. The periodic slab calculations performed by us and also from an earlier study[60] showed that this excess charge density is delocalized over all the Ti atoms located in the top two layers. The PEEC model used here cannot reproduce such symmetric delocalization of charge density because of restrictions applied to the cluster model. Here, the excess charge density is delocalized over the Ti atoms mostly in the subsurface layer, especially on Ti atoms that are close to the ECPs and point charges, which results in larger adsorption energies. A similar explanation holds for the reduced system where the excess charge density in the $Ti_{46}O_{91}$ cluster is delocalized over the subsurface Ti atomic layers of the cluster. When the metal cluster makes a covalent bond to the Ti atoms at the vacant site, as in the case of Pt_2 and Au_3 clusters, the adsorption energy for the reduced cluster is increased by about 0.4 eV. For Au_2 and Pt_3 clusters, the adsorption energy is again within 0.3 eV to results from periodic slab calculations. However, we argue here that the delocalization of the excess charge density over all Ti atoms on the surface is unphysical and is a result of the self-interaction error of GGA-DFT functionals. In contrast, computations with hybrid PBE0 functional predict, in our opinion, more physical electronic structures that show localization of the excess charge density on one Ti atom on the TiO_2 surface in the case of the Au_3 complex on the stoichiometric surface and on the Ti atoms neighboring the oxygen vacancy in the case of the reduced cluster. In other words, we expect the PEEC model when used together with hybrid PBE0 functional to compute more accurate adsorption energies for systems with unpaired electrons.

On the stoichiometric surface, adsorption energies calculated with the PBE0 functional are for all studied metal clusters quite similar to those obtained with PBE functional. However, the PBE0 functional predicts a stronger adsorption for all metal clusters on the reduced surface compared to the PBE functional. As mentioned above, the reduced cluster ($Ti_{46}O_{91}$) optimized with PBE0 functional has the excess charge density localized at the vacant site and thus predicts a higher energy due to repulsive interaction between the two unpaired electrons. Adsorption of metal clusters at this site either use these electrons to form covalent bonds or move them to the Ti atoms in the subsurface layer in TiO_2 (110) (in the case of $Au_2/Ti_{46}O_{91}$) to minimize the repulsive interaction. The energy gained due to the adsorption of metal clusters on the reduced TiO_2 (110) surface is therefore larger if computed with PBE0 functional as compared to PBE functional.

The selected structural parameters for all complexes optimized with PBE0 functional are shown in Fig. 5. In general, Pt clusters interact more strongly with both the stoichiometric and the reduced TiO_2 surfaces than Au clusters. The Pt–Pt bond distance in the adsorbed Pt_2 complexes is longer than the Pt–Pt bond distance (2.52 Å) in the gas phase. In contrast, for adsorbed Au_2 complexes no significant change in the Au–Au bond distance is observed (d_{Au-Au}=2.55 Å) compared to the gas phase molecule. The stronger Pt_n adsorption also results in shorter Pt–Ti_{5c}, Pt–O_{br}, and Pt–O_s distances when compared to the corresponding distances in the Au_n complexes. Au clusters do not exhibit any interaction with the O_s atoms on the TiO_2 surface. Comparing the interaction of Pt_2 and Pt_3 with the TiO_2 surface, differences in the bond distances suggest a slightly weaker interaction for Pt_3. The smaller cluster has more undercoordinated metal atoms and therefore interacts more strongly with the surface. In contrast, the interaction of Au_3 with the TiO_2 surface is stronger than for Au_2 due to the presence of an unpaired electron in the Au_3 complex, which facilitates charge transfer from Au_3 to the TiO_2 surface.

B. Charge transfer between adsorbed (M_n) clusters and the TiO_2 (110) surface

Metal atom adsorption on an oxide surface is accompanied by charge transfer between the metal and the oxide surface affecting the oxidation state of the adsorbed metal atoms. The oxidation state of the metal atoms is believed to be closely linked to their catalytic activity for many important industrial reactions, such as the WGS reaction, and there is an intense debate in literature on the nature of the active metal atoms, i.e., whether they are cationic, anionic, or metallic.[10,71,72] In this section, we investigate the oxidation state of metal clusters on the TiO_2 (110) surface by compar-

TABLE VI. The calculated charges (e) on the metal cluster at the M_n/TiO_2 (110) interface.

		$q(M_n)$				
			PEECM ($Ti_{46}O_{92}$)			
		Periodic slab (PBE)	PBE		PBE0	
Surface	Metal cluster	Bader	Bader	NPA	Bader	NPA
TiO_2	Au_2	0.10	0.35	0.79	0.33	0.78
	Au_3	0.59	0.79	1.02	0.82	1.03
	Pt_2	0.20	0.36	0.92	0.36	0.89
	Pt_3	0.32	0.56	1.04	0.47	0.96
TiO_{2-x}	Au_2	−0.04	0.27	0.64	0.25	0.64
	Au_3	−0.39	−0.07	0.70	−0.10	0.70
	Pt_2	−0.54	−0.30	0.44	−0.40	0.34
	Pt_3	−0.25	0.04	0.85	−0.14	0.71

ing the amount of charge transfer between the metal clusters and the surface. The total electronic charge on the metal clusters, $q(M_n)$, calculated with different methodologies are presented in Table VI. For periodic slab models using Bader's charge analysis,[73] the calculated Au cluster charges are in close agreement with the previously reported values.[60,67] There is no significant charge transfer between Au_2 and the stoichiometric TiO_2 (110) surface consistent with the weak interaction between Au_2 and the surface. In contrast, Au_3 transfers a significant amount of charge (0.59 e) to the TiO_2 surface due to the presence of an unpaired electron in its high-energy singly occupied molecular orbital. For Pt_2/TiO_2 and Pt_3/TiO_2 complexes, the adsorbed clusters have positive charges (+0.20 and +0.32, respectively), indicating again some charge transfer between the occupied orbitals of the metal cluster and the unoccupied Ti 3*d*-orbitals and explaining the shorter metal-Ti distances for Pt clusters in comparison to Au clusters displayed in Fig. 5.

For the reduced surface, the oxygen vacancy is believed to be an electron donor site due to excess charge density left behind when the bridging oxygen atom is removed from the surface. Thus, metal atoms at this vacant site become negatively charged due to electron transfer from the surface. Bader charges on the metal atoms (calculated from periodic slab models) are negative except for the Au_2 cluster. The absence of a net charge transfer from the reduced surface to Au_2 can be understood from the lowest energy structure of Au_2/TiO_{2-x} (Fig. 5) that has both Au atoms positioned at the vacant site interacting weakly with the neighboring bridging oxygen atoms.

Next, we discuss the Bader charges for the PEEC models calculated with both PBE and PBE0 functionals. Table VI illustrates that the Bader charges on the metal clusters are independent of the functional quite similar and about 0.2 electron more positive than the corresponding charges obtained from the periodic slab models. This trend is in agreement with the slightly larger adsorption energies predicted by the PEEC models compared to the periodic slab models. Also, for adsorbed metal clusters on the reduced surface, we observe, except for Au_2, a negative charge with magnitude slightly smaller than the one obtained from the periodic slab models.

Considering the ongoing debate in literature on the charge state of the metal atoms, we also computed NPA charges and Mulliken charges for the PEEC models. In the following, we only discuss NPA charges; the Mulliken charges are qualitatively identical to NPA charges. Table VI illustrates that NPA charges on the metal clusters are consistently more positive than Bader charges. Nevertheless, the relative trends in net charge transfer between the metal clusters and the oxide surfaces are in good agreement with our Bader charge analysis. It is still important to note that the NPA charges of the metal clusters adsorbed on the reduced surface are consistently positive, contrary to our Bader charge analysis. To further investigate this phenomenon, Table VII illustrates the charges on individual metal atoms for the very negatively charged (Bader analysis) Pt_2/TiO_{2-x} and Au_3/TiO_{2-x} complexes using different methodologies. Bader charges for the metal atoms directly adsorbed at the vacancy [Pt(1) and Au(1)] are very similar for the PEEC and periodic slab models and are independent of DFT functional. In contrast, natural population analysis predicts that the Pt(1) in Pt_2/TiO_{2-x} and the Au(1) in Au_3/TiO_{2-x} display a metallic or even a cationic behavior. Overall, the question remains whether the metal atoms adsorbed on the reduced TiO_2 (110) surface are truly negatively charged? We only note here that Cramer[74] has previously discussed different charge models and concluded that Bader charges should not be used for analysis whenever the lower atomic multipole moments are quantitatively important as they likely will be for the reduced TiO_{2-x} surface. We will further discuss the oxidation state of metal atoms adsorbed at oxygen vacancies in a future study.

C. Binding mechanism and orbital overlap between (M_n) clusters and the TiO_2 (110) surface

To shed more light on the origin of the differences in the adsorption behavior of Au_n and Pt_n clusters, we have analyzed the electronic structure changes accompanying the adsorption of Au_2 and Pt_2. The total DOS and the atom-projected DOS for adsorbed Au_2 and Pt_2 on the stoichiometric TiO_2 (110) surface are shown in Figs. 6(a) and 6(c), respectively. We note that the DOS calculated with the PBE functional (not shown) for the adsorbed Pt_2 and Pt_3

TABLE VII. The calculated charges (e) on individual metal atoms for selected M_n/TiO_{2-x} (110) systems.

		q(M)				
			PEECM ($Ti_{46}O_{92}$)			
		Periodic slab (PBE)	PBE		PBE0	
Surface	Metal atoms adsorbed on the oxygen vacancy[a]	Bader	Bader	NPA	Bader	NPA
$TiO_{2-x}\cdots Pt_2$	Pt(1)	−0.31	−0.25	0.20	−0.32	0.12
	Pt(2)	−0.23	−0.05	0.24	−0.08	0.22
$TiO_{2-x}\cdots Au_3$	Au(1)	−0.32	−0.22	0.07	−0.24	0.06
	Au(2)	−0.05	0.01	0.23	0.07	0.24
	Au(3)	−0.02	0.14	0.40	0.08	0.40

[a]Metal atoms are numbered based on their distance from the oxygen vacancy site. M(1) is adsorbed at the vacancy site.

clusters on both the stoichiometric and reduced surfaces displays no band gap, indicating metallization of the system. In contrast, hybrid DFT calculations suggest the presence of metal states in the band gap close to the Fermi level. These states are known as metal induced gap states (MIGS)[66,70,75] as they appear in the band gap of the clean TiO_2 (110) surface. Figure 6(a) indicates that these MIGS emerged from the molecular Au_2 orbitals with no mixing with the O 2*p* states. The corresponding molecular orbital pictures [see Fig. 6(b)] illustrate that the Au–O interaction is thus a weak filled-filled interaction. In the case of the Pt_2 complex, the Pt *d* states at the Fermi level are closer to the conduction band [about 2 eV apart; Fig. 6(c)] than the corresponding states in the Au_2 complex [about 2.6 eV apart; Fig. 6(a)]. A strong overlap between the Pt and TiO_2 molecular orbitals [see Fig. 6(d)] is observed, indicating localized covalent bonding between Pt and oxygen atoms enabled by nearby Ti-centered electron-accepting empty states. The molecular orbitals corresponding to the remaining MIGS not shown in Figs. 6(b) and 6(d) originate primarily from pure Au or Pt *d* orbitals.

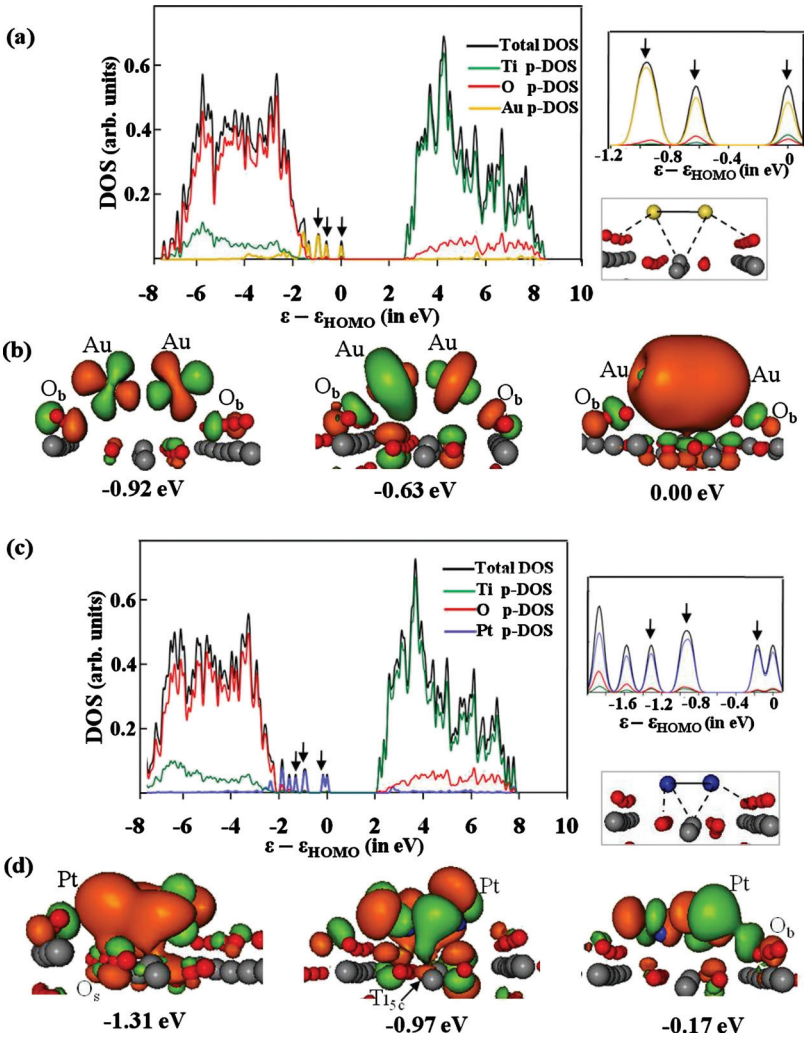

FIG. 6. [(a) and (c)] The total and partial DOS of (a) Au_2 and (c) Pt_2 adsorbed on the stoichiometric TiO_2 (110) surface computed with the PEEC methodology using the PBE0 functional ($Ti_{46}O_{92}$ cluster). Projections of the MIGS are shown on the right side of the DOS plots. [(b) and (d)] The selected occupied molecular orbitals corresponding to the interaction of (b) Au_2 and (d) Pt_2 on $Ti_{46}O_{92}$ (indicated by arrows in the DOS plots). The energies shown under each molecular orbital are relative to the corresponding HOMO energy. The isosurfaces are colored according to the sign of the wave function and drawn for 0.02 $e/Å^3$.

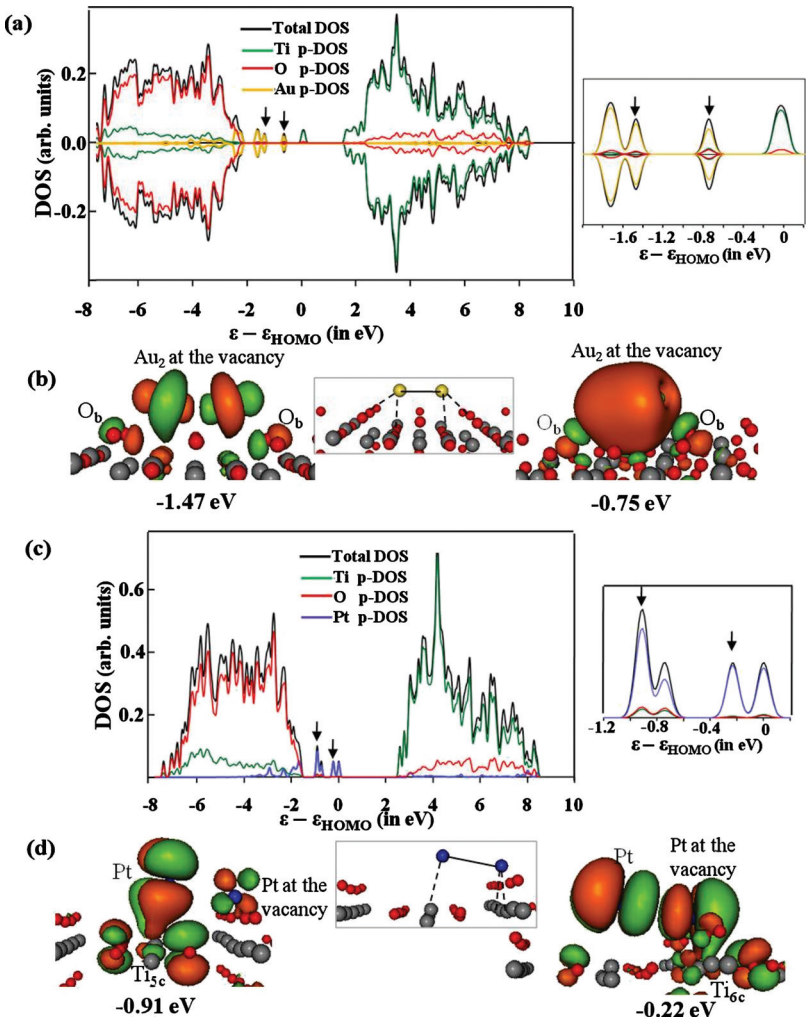

FIG. 7. [(a) and (c)] The total and partial DOS of (a) Au_2 and (c) Pt_2 adsorbed on the reduced TiO_2 (110) surface computed with the PEEC methodology using the PBE0 functional ($Ti_{46}O_{91}$ cluster). Projections of the MIGS are shown on the right side of the DOS plots. [(b) and (d)] The selected occupied molecular orbitals corresponding to the interaction of (b) Au_2 and (d) Pt_2 on $Ti_{46}O_{91}$ (indicated by arrows in the DOS plots). The energies shown under each molecular orbital are relative to the corresponding HOMO energy. The isosurfaces are colored according to the sign of the wave function and drawn for 0.02 $e/Å^3$.

The type of interaction of both Au_2 and Pt_2 clusters with the reduced surface is slightly different from that of the stoichiometric surface. While Au_2 places both Au atoms at the vacant site making overlaps with the neighboring bridging oxygen atoms, as shown in Fig. 5(b), Pt_2 places only one Pt atom at the vacant site making a strong interaction with the two Ti atoms neighboring the vacancy and the other Pt atom interacting with the Ti_{5c} atom [see Fig. 5(d)]. The excess charge density originally localized on the two Ti atoms neighboring the oxygen vacancy is not used for the Au_2/TiO_{2-x} interaction, it remains on the surface. DOS calculated for Au_2/TiO_{2-x} shown in Fig. 7(a) indicates that the gap state near the Fermi energy corresponds to charge density localized on two Ti atoms in the subsurface layer of the surface. The remaining gap states originate mainly from Au_2 molecular orbitals. The molecular orbitals shown in Fig. 7(b) confirm that the high-energy molecular orbitals of Au_2/TiO_{2-x} are combinations of the eigenstates of Au_2 and orbitals localized on the bridging and surface oxygen atoms. In contrast, for the Pt_2/TiO_{2-x} system, the DOS shown in Fig. 7(c) and the molecular orbital diagrams shown in Fig. 7(d) illustrate that the excess charge density left on the reduced surface is used to form covalent bond type interactions between the Pt_2 cluster and the surface. Here, the frontier molecular orbitals originate from the interaction of the HOMOs of the Pt_2 molecule and the Ti $3d$ orbitals. Thus, a stronger interaction of Pt_2 with the stoichiometric and reduced surfaces involves both surface Ti and O atoms, while Au_2 interacts only weakly with the TiO_2 surface through the oxygen atoms.

V. REDUCIBILITY OF THE TiO_2 SURFACE

One key aspect in the study of metal-surface interactions is the effect of metal deposition on the reducibility of the surface. Earlier studies revealed that metal deposition on the TiO_2 surface is accompanied by a strong polarization of the adsorbed atoms, which eventually leads to electron density transfer to the surface. Recent studies on oxide supported Au and Pt catalysts for the WGS reaction indicate that the role of the dispersed metallic phase is not restricted to providing sites for CO adsorption, but that it furthermore affects the reducibility of the support, thereby creating new active sites for the WGS reaction.[71,76] We have investigated this hypothesis by calculating the oxygen vacancy formation energies (E_{vf}) in the presence and absence of metal clusters. We used the following equation to calculate E_{vf} in the presence of metal clusters:

$$E_{vf}[M_n] = E_{vf}[\text{clean}] + E_{ads}[M_n/\text{R-TiO}_2] - E_{ads}[M_n/\text{S-TiO}_2], \quad (4)$$

where $E_{ads}[M_n/\text{R-TiO}_2]$ and $E_{ads}[M_n/\text{S-TiO}_2]$ are the BSSE

TABLE VIII. Effect of metal clusters on the oxygen vacancy formation energy (E_{vf}) of the rutile TiO_2 (110) surface.

	E_{vf} (eV)[a]		
	VASP	PEECM ($Ti_{46}O_{92}$)	
Surface	PBE	PBE	PBE0
TiO_2	3.76	3.75	4.37
$TiO_2\cdots Au_2$	3.51	3.83	3.62
$TiO_2\cdots Au_3$	3.32	3.77	4.15
$TiO_2\cdots Pt_2$	2.25	2.12	2.10
$TiO_2\cdots Pt_3$	2.87	3.16	3.11

[a]E_{vf} [M_n] is calculated using Eq. (4).

corrected adsorption energies of M_n on the reduced and stoichiometric TiO_2 (110) surfaces, respectively. The calculated E_{vf} values using both periodic slab and PEEC models are illustrated in Table VIII. The PEECM and periodic slab model calculations with PBE functional result in very similar E_{vf} values, indicating the ability of PEEC models to reproduce reaction energies obtained from periodic slab calculations. As mentioned earlier in Sec. III B, the oxygen vacancy formation energy calculated with PBE0 functional for the clean surface is about 0.6 eV higher than the one obtained with PBE functional. This energy difference arises from the different electronic structures obtained with the two functionals for the reduced surface.

In general, Pt clusters promote a stronger reducibility of the TiO_2 surface than the Au clusters. PBE functional computations indicate that Au clusters do not have any significant effect on the reducibility of the TiO_2 surface. However, hybrid DFT calculations reveal that the Au clusters may help reduce the TiO_2 surface by about 0.7 and 0.2 eV for the Au_2 and Au_3 clusters, respectively. The effect of reducibility decreases with an increase in the metal cluster size due to the stronger adsorption of smaller clusters on the reduced surface. The enhanced reducibility of the TiO_2 surface in the presence of metal clusters can, in general, be attributed to the formation of MIGS induced by metal cluster adsorption. These MIGS offer states suitable for accommodating extra electrons and facilitate the reduction. In the case of Pt adsorption, this leads to the formation of MIGS at the Fermi energy that are quite close to the conduction band [in comparison to Au adsorption, see Figs. 6(a) and 6(c)] so that the oxygen vacancy formation energy is reduced by as much as 1–2 eV.

VI. CONCLUSIONS

The metal/TiO_2 interface has been investigated for small Au and Pt clusters using the periodic slab and PEEC models. Both methodologies predict similar metal adsorption and oxygen vacancy formation energies, with the PEEC methodology being significantly more efficient if hybrid exchange functionals are used. Tests on the effect of different DFT functionals, including the double-hybrid B2PLYP functional, indicate that the GGA-PBE functional is able to predict the strong Pt adsorption energy on the stoichiometric TiO_2 surface fairly accurately, while the popular B3LYP functional seems to underestimate the Pt adsorption energy by about 0.5 eV. In contrast, reasonable electronic structures cannot be obtained with the GGA-PBE functional. PEECM computations with hybrid PBE0 functional result in more physical electronic structures with wider band gaps. Particularly for the reduced TiO_2 surface, the excess charge produced by reducing the surface is fully localized on the Ti atoms neighboring the vacancy if the PBE0 functional is used, while it is delocalized if the GGA-PBE functional is used. This difference in the electronic structure is found to be important for metal cluster adsorption on the reduced TiO_2 surface and for the effect of metal clusters on the reducibility of the TiO_2 surface. Hybrid PBE0 calculations predict that the oxygen vacancy formation energy decreases by about 1.2–2.2 eV in the presence of Pt clusters and by about 0.2–0.7 eV in the presence of Au clusters. In contrast, GGA-PBE calculations predict that the oxygen vacancy formation energy decreases only by 0.9–1.5 eV in the presence of Pt clusters and by 0.2–0.4 eV in the presence of Au clusters. The effect is more pronounced for Pt clusters since Pt makes a strong covalent type interaction with the TiO_2 surface, while Au makes only a weak filled-filled type interaction with TiO_2.

ACKNOWLEDGMENTS

Helpful discussions with Asbjörn Burow are acknowledged. This work was supported by the National Science Foundation under Grant No. CBET-0932991 and in part by TeraGrid resources provided by the National Center for Supercomputing Applications (NCSA), Louisiana Optical Network Initiative (LONI), and the Purdue University under Grant No. TG-CTS090100. Furthermore, a portion of this research was performed at the Center for Nanophase Materials Sciences, which is sponsored at Oak Ridge National Laboratory by the Division of Scientific User Facilities, U.S. Department of Energy (Grant No. CNMS2009-248) and at EMSL, a national scientific user facility sponsored by the Department of Energy's Office of Biological and Environmental Research located at Pacific Northwest National Laboratory (Grant Proposal No. 34900). Finally, computing resources from the USC NanoCenter, USC's High Performance Computing Group, and the Minnesota Supercomputing Institute for Advanced Computational Research are gratefully acknowledged.

[1] B. C. Gates, Chem. Rev. (Washington, D.C.) **95**, 511 (1995); D. W. Goodman, *ibid.* **95**, 523 (1995); *Chemisorption and Reactivity on Supported Clusters and Thin Films: Towards an Understanding of Microscopic Processes in Catalysis*, edited by R. M. Lambert and G. Pacchioni (Kluwer, Dordrecht, 1997).
[2] M. Haruta, Catal. Today **36**, 153 (1997); Nature (London) **437**, 1098 (2005).
[3] M. Valden, X. Lai, and D. W. Goodman, Science **281**, 1647 (1998).
[4] A. S. K. Hashmi and G. J. Hutchings, Angew. Chem., Int. Ed. **45**, 7896 (2006); G. J. Hutchings, M. Brust, and H. Schmidbaur, Chem. Soc. Rev. **37**, 1759 (2008).
[5] M. Haruta, N. Yamada, T. Kobayashi, and S. Iijima, J. Catal. **115**, 301 (1989); G. C. Bond and D. T. Thompson, Catal. Rev. - Sci. Eng. **41**, 319 (1999).
[6] M. Haruta, Gold Bull. **37**, 27 (2004).
[7] M. Haruta and M. Date, Appl. Catal., A **222**, 427 (2001); T. Hayashi, K. Tanaka, and M. Haruta, J. Catal. **178**, 566 (1998); G. Mul, A. Zwijnenburg, B. van der Linden, M. Makkee, and J. A. Moulijn, *ibid.* **201**, 128

(2001); E. E. Stangland, K. B. Stavens, R. P. Andres, and W. N. Delgass, *ibid.* **191**, 332 (2000); C. J. Crump, J. D. Gilbertson, and B. D. Chandler, Top. Catal. **49**, 233 (2008); Q. Y. Li, K. Wang, S. L. Zhang, M. Zhang, H. J. Yang, and Z. S. Jin, J. Mol. Catal. A: Chem. **258**, 83 (2006); C. B. Zhang, H. He, and K. Tanaka, Catal. Commun. **6**, 211 (2005).
[8] C. Mohr, N. Hofmeister, M. Lucas, and P. Claus, Chem. Eng. Technol. **23**, 324 (2000); T. V. Choudhary, C. Sivadinarayana, A. K. Datye, D. Kumar, and D. W. Goodman, Catal. Lett. **86**, 1 (2003); M. Boronat, P. Concepcion, A. Corma, S. Gonzalez, F. Illas, and P. Serna, J. Am. Chem. Soc. **129**, 16230 (2007); X. X. Han, R. X. Zhou, G. H. Lai, B. H. Yue, and X. M. Zheng, J. Mol. Catal. A: Chem. **209**, 83 (2004); A. Dandekar and M. A. Vannice, J. Catal. **183**, 344 (1999).
[9] F. Boccuzzi, A. Chiorino, and M. Manzoli, Surf. Sci. **502–503**, 513 (2002); A. Sandoval, A. Gomez-Cortes, R. Zanella, G. Diaz, and J. M. Saniger, J. Mol. Catal. A: Chem. **278**, 200 (2007); G. P. Wu, T. Chen, W. G. Su, G. H. Zhou, X. Zong, Z. B. Lei, and C. Li, Int. J. Hydrogen Energy **33**, 1243 (2008); H. Iida and A. Igarashi, Appl. Catal., A **298**, 152 (2006); K. G. Azzam, I. V. Babich, K. Seshan, and L. Lefferts, J. Catal. **251**, 153 (2007); **251**, 163 (2007); C. M. Kalamaras, P. Panagiotopoulou, D. I. Kondarides, and A. M. Efstathiou, *ibid.* **264**, 117 (2009); J. A. Rodríguez, J. Evans, J. Graciani, J. B. Park, P. Liu, J. Hrbek, and J. F. Sanz, J. Phys. Chem. C **113**, 7364 (2009).
[10] R. Burch, Phys. Chem. Chem. Phys. **8**, 5483 (2006).
[11] E. Dokou, E. E. Stangland, R. P. Andres, W. N. Delgass, and M. A. Barteau, Catal. Lett. **70**, 1 (2000).
[12] S. Kielbassa, M. Kinne, and R. J. Behm, J. Phys. Chem. B **108**, 19184 (2004).
[13] S. Ichikawa, T. Akita, M. Okumura, M. Haruta, K. Tanaka, and M. Kohyama, J. Electron Microsc. **52**, 21 (2003).
[14] Y. S. Su, M. Y. Lee, and S. D. Lin, Catal. Lett. **57**, 49 (1999); J. Ruiz-Martínez, A. Sepúlveda-Escribano, J. A. Anderson, and F. Rodríguez-Reinoso, Phys. Chem. Chem. Phys. **11**, 917 (2009); S. Lee, C. Y. Fan, T. P. Wu, and S. L. Anderson, Surf. Sci. **578**, 5 (2005); J. Chem. Phys. **123**, 124710 (2005); T. P. Wu, W. E. Kaden, and S. L. Anderson, J. Phys. Chem. C **112**, 9006 (2008).
[15] K. D. Schierbaum, S. Fischer, M. C. Torquemada, J. L. deSegovia, E. Roman, and J. A. MartinGago, Surf. Sci. **345**, 261 (1996).
[16] O. Ozturk, J. B. Park, S. Ma, J. S. Ratliff, J. Zhou, D. R. Mullins, and D. A. Chen, Surf. Sci. **601**, 3099 (2007).
[17] Y. M. Shul'ga, A. Y. Stakheev, N. S. Telegina, O. N. Tkachenko, and K. M. Minachev, Dokl. Phys. Chem. **379**, 199 (2001).
[18] T. Akita, P. Lu, S. Ichikawa, K. Tanaka, and M. Haruta, Surf. Interface Anal. **31**, 73 (2001).
[19] S. Fischer, K. D. Schierbaum, and W. Gopel, Vacuum **48**, 601 (1997); N. Isomura, X. Y. Wu, and Y. Watanabe, J. Chem. Phys. **131**, 164707 (2009); R. Lazzari, G. Renaud, J. Jupille, and F. Leroy, Phys. Rev. B **76**, 125412 (2007); X. Tong, L. Benz, S. Chretien, H. Metiu, M. T. Bowers, and S. K. Buratto, J. Phys. Chem. C **114**, 3987 (2010); X. Tong, L. Benz, P. Kemper, H. Metiu, M. T. Bowers, and S. K. Buratto, J. Am. Chem. Soc. **127**, 13516 (2005).
[20] O. Dulub, W. Hebenstreit, and U. Diebold, Phys. Rev. Lett. **84**, 3646 (2000).
[21] S. J. Tauster, Acc. Chem. Res. **20**, 389 (1987); W. X. Xu, K. D. Schierbaum, and W. Goepel, J. Solid State Chem. **119**, 237 (1995); F. Pesty, H. P. Steinruck, and T. E. Madey, Surf. Sci. **339**, 83 (1995); D. R. Jennison, O. Dulub, W. Hebenstreit, and U. Diebold, *ibid.* **492**, L677 (2001); A. K. Datye, D. S. Kalakkad, M. H. Yao, and D. J. Smith, J. Catal. **155**, 148 (1995).
[22] L. Zhang, R. Persaud, and T. E. Madey, Phys. Rev. B **56**, 10549 (1997).
[23] G. Pacchioni, J. Chem. Phys. **128**, 182505 (2008); J. L. F. Da Silva, M. V. Ganduglia-Pirovano, J. Sauer, V. Bayer, and G. Kresse, Phys. Rev. B **75**, 045121 (2007).
[24] C. Di Valentin, G. Pacchioni, and A. Selloni, Phys. Rev. Lett. **97**, 166803 (2006).
[25] A. M. Burow, M. Sierka, J. Dobler, and J. Sauer, J. Chem. Phys. **130**, 174710 (2009).
[26] R. Ahlrichs, M. Bar, M. Haser, H. Horn, and C. Kolmel, Chem. Phys. Lett. **162**, 165 (1989); O. Treutler and R. Ahlrichs, J. Chem. Phys. **102**, 346 (1995).
[27] C. G. Lambert, T. A. Darden, and J. A. Board, J. Comput. Phys. **126**, 274 (1996); K. N. Kudin and G. E. Scuseria, Chem. Phys. Lett. **283**, 61 (1998); J. Chem. Phys. **121**, 2886 (2004).
[28] C. M. Yim, C. L. Pang, and G. Thornton, Phys. Rev. Lett. **104**, 259704 (2010); S. Wendt, P. T. Sprunger, E. Lira, G. K. H. Madsen, Z. S. Li, J. O. Hansen, J. Matthiesen, A. Blekinge-Rasmussen, E. Laegsgaard, B. Hammer, and F. Besenbacher, Science **320**, 1755 (2008).
[29] J. Muscat, A. Wander, and N. M. Harrison, Chem. Phys. Lett. **342**, 397 (2001); T. Bredow and G. Pacchioni, *ibid.* **355**, 417 (2002).
[30] C. Di Valentin, G. Pacchioni, and A. Selloni, J. Phys. Chem. C **113**, 20543 (2009).
[31] B. J. Morgan and G. W. Watson, Surf. Sci. **601**, 5034 (2007).
[32] G. Kresse and J. Furthmuller, Phys. Rev. B **54**, 11169 (1996); G. Kresse and J. Hafner, *ibid.* **47**, 558 (1993); **49**, 14251 (1994); G. Kresse and J. Furthmuller, Comput. Mater. Sci. **6**, 15 (1996).
[33] J. P. Perdew, K. Burke, and M. Ernzerhof, Phys. Rev. Lett. **77**, 3865 (1996).
[34] G. Makov and M. C. Payne, Phys. Rev. B **51**, 4014 (1995).
[35] J. Harris, Phys. Rev. B **31**, 1770 (1985); W. Matthew C. Foulkes and R. Haydock, *ibid.* **39**, 12520 (1989).
[36] J. P. Perdew and Y. Wang, Phys. Rev. B **45**, 13244 (1992).
[37] J. P. Perdew, M. Emzerhof, and K. Burke, J. Chem. Phys. **105**, 9982 (1996).
[38] B. I. Dunlap, J. W. D. Connolly, and J. R. Sabin, J. Chem. Phys. **71**, 3396 (1979); K. Eichkorn, O. Treutler, H. Ohm, M. Haser, and R. Ahlrichs, Chem. Phys. Lett. **242**, 652 (1995).
[39] TURBOMOLE, version 6.0, University of Karlsruhe and Forschungszentrum Karlsruhe GmbH, 2009.
[40] P. J. Hay and W. R. Wadt, J. Chem. Phys. **82**, 270 (1985).
[41] T. Bredow and G. Pacchioni, Surf. Sci. **426**, 106 (1999).
[42] L. Giordano, G. Pacchioni, T. Bredow, and J. F. Sanz, Surf. Sci. **471**, 21 (2001).
[43] J. F. Sanz, N. C. Hernandez, and A. Marquez, Theor. Chem. Acc. **104**, 317 (2000).
[44] A. Schäfer, C. Huber, and R. Ahlrichs, J. Chem. Phys. **100**, 5829 (1994).
[45] D. Andrae, U. Haussermann, M. Dolg, H. Stoll, and H. Preuss, Theor. Chim. Acta **77**, 123 (1990).
[46] S. F. Boys and F. Bernardi, Mol. Phys. **19**, 553 (1970).
[47] S. Kurth, J. P. Perdew, and P. Blaha, Int. J. Quantum Chem. **75**, 889 (1999).
[48] J. K. Nørskov, J. Rossmeisl, A. Logadottir, L. Lindqvist, J. R. Kitchin, T. Bligaard, and H. Jónsson, J. Phys. Chem. B **108**, 17886 (2004).
[49] P. W. Atkins, *Physical Chemistry*, 6th ed. (Oxford University Press, Oxford, 1998).
[50] J. A. Pople, M. Headgordon, D. J. Fox, K. Raghavachari, and L. A. Curtiss, J. Chem. Phys. **90**, 5622 (1989).
[51] H. Iddir, S. Ogut, N. D. Browning, and M. M. Disko, Phys. Rev. B **72**, 081407 (2005); **73**, 039902(E) (2006).
[52] H. Iddir, V. Skavysh, S. Ogut, N. D. Browning, and M. M. Disko, Phys. Rev. B **73**, 041403 (2006).
[53] A. E. Reed, R. B. Weinstock, and F. Weinhold, J. Chem. Phys. **83**, 735 (1985).
[54] P. Reinhardt, M. Causa, C. M. Marian, and B. A. Hess, Phys. Rev. B **54**, 14812 (1996).
[55] A. D. Becke, Phys. Rev. A **38**, 3098 (1988); C. T. Lee, W. T. Yang, and R. G. Parr, Phys. Rev. B **37**, 785 (1988).
[56] T. Schwabe and S. Grimme, Phys. Chem. Chem. Phys. **9**, 3397 (2007); F. Neese, T. Schwabe, and S. Grimme, J. Chem. Phys. **126**, 124115 (2007); T. Schwabe and S. Grimme, Phys. Chem. Chem. Phys. **8**, 4398 (2006).
[57] M. Piacenza, I. Hyla-Kryspin, and S. Grimme, J. Comput. Chem. **28**, 2275 (2007); T. Schwabe and S. Grimme, Acc. Chem. Res. **41**, 569 (2008).
[58] A. D. Becke, J. Chem. Phys. **98**, 5648 (1993).
[59] R. Huenerbein, B. Schirmer, J. Moellmann, and S. Grimme, Phys. Chem. Chem. Phys. **12**, 6940 (2010); T. Schwabe and S. Grimme, J. Phys. Chem. Lett. **1**, 1201 (2010); S. Grimme and J. P. Djukic, Inorg. Chem. **49**, 2911 (2010).
[60] S. Chrétien and H. Metiu, J. Chem. Phys. **127**, 244708 (2007).
[61] X. Y. Wu, A. Selloni, and S. K. Nayak, J. Chem. Phys. **120**, 4512 (2004).
[62] A. Vijay, G. Mills, and H. Metiu, J. Chem. Phys. **118**, 6536 (2003); M. D. Rasmussen, L. M. Molina, and B. Hammer, *ibid.* **120**, 988 (2004); K. J. Hameeuw, G. Cantele, D. Ninno, F. Trani, and G. Iadonisi, *ibid.* **124**, 024708 (2006); S. J. Thompson and S. P. Lewis, Phys. Rev. B **73**, 073403 (2006); T. Bredow, L. Giordano, F. Cinquini, and G. Pacchioni, *ibid.* **70**, 035419 (2004).
[63] R. L. Kurtz, R. Stockbauer, T. E. Madey, E. Roman, and J. L. Desegovia, Surf. Sci. **218**, 178 (1989); M. A. Henderson, W. S. Epling, C. H. F. Peden, and C. L. Perkins, J. Phys. Chem. B **107**, 534 (2003).
[64] J. G. Wang and B. Hammer, Phys. Rev. Lett. **97**, 136107 (2006); D.

Pillay and G. S. Hwang, J. Mol. Struct.: THEOCHEM **771**, 129 (2006); Phys. Rev. B **72**, 205422 (2005); D. Matthey, J. G. Wang, S. Wendt, J. Matthiesen, R. Schaub, E. Laegsgaard, B. Hammer, and F. Besenbacher, Science **315**, 1692 (2007); Y. Wang and G. S. Hwang, Surf. Sci. **542**, 72 (2003).
[65] G. K. H. Madsen and B. Hammer, J. Chem. Phys. **130**, 044704 (2009).
[66] N. Lopez and J. K. Norskov, Surf. Sci. **515**, 175 (2002).
[67] S. Chrétien and H. Metiu, J. Chem. Phys. **127**, 084704 (2007).
[68] T. Pabisiak and A. Kiejna, Phys. Rev. B **79**, 085411 (2009).
[69] Y. Han, C. J. Liu, and Q. F. Ge, J. Phys. Chem. C **111**, 16397 (2007); E. Mete, D. Uner, O. Gulseren, and S. Ellialtioglu, Phys. Rev. B **79**, 125418 (2009).
[70] Y. Han, C. J. Liu, and Q. F. Ge, J. Phys. Chem. B **110**, 7463 (2006).
[71] Q. Fu, W. L. Deng, H. Saltsburg, and M. Flytzani-Stephanopoulos, Appl. Catal., B **56**, 57 (2005); Q. Fu, H. Saltsburg, and M. Flytzani-Stephanopoulos, Science **301**, 935 (2003).
[72] D. Tibiletti, A. Amieiro-Fonseca, R. Burch, Y. Chen, J. M. Fisher, A. Goguet, C. Hardacre, P. Hu, and A. Thompsett, J. Phys. Chem. B **109**, 22553 (2005).
[73] R. F. W. Bader, *Atoms in Molecules: A Quantum Theory* (Clarendon, Oxford, 1990).
[74] C. J. Cramer, *Essentials of Computational Chemistry: Theories and Models* (Wiley, West Sussex, 2007), Chap. 9.
[75] T. Tamura, S. Ishibashi, K. Terakura, and H. M. Weng, Phys. Rev. B **80**, 195302 (2009).
[76] Y. Chen, P. Crawford, and P. Hu, Catal. Lett. **119**, 21 (2007); A. Goguet, F. Meunier, J. P. Breen, R. Burch, M. I. Petch, and A. F. Ghenciu, J. Catal. **226**, 382 (2004).